

# Symmetry selection rules for the intrinsic nonlinear thermal Hall effect in altermagnets: Role of quantum metric and $C_2$ rotational symmetry

Gunn Kim<sup>1</sup>

<sup>1</sup>*Department of Physics, Sejong University, Seoul 05006, South Korea*  
(Dated: March 5, 2026)

We establish symmetry-based selection rules for the intrinsic nonlinear thermal Hall effect driven by the quantum metric in altermagnets. We show that a nonvanishing nonlinear thermal Hall conductivity  $\kappa_{xyy}$  requires three conditions: (i) a nontrivial quantum metric, (ii) breaking of mirror symmetry  $M_x$ , and (iii) breaking of twofold rotational symmetry  $C_2$ . Using tight-binding models on a square lattice, we demonstrate that  $d$ -wave altermagnets naturally break  $C_2$  through parity-mixing orbital hybridizations, while  $g$ -wave systems preserve  $C_2$ , forcing the response to vanish identically. Step-by-step Taylor expansions and explicit unitary matrix proofs establish these results. Our framework provides predictive power for material selection and lays the groundwork for nonlinear spin-caloritronic devices.

## I. INTRODUCTION

Altermagnets represent a newly identified magnetic phase characterized by collinear antiferromagnetic order that supports strong, momentum-dependent spin splitting without macroscopic time-reversal symmetry breaking [1–7]. Unlike conventional antiferromagnets where Kramers degeneracy is enforced globally, the unique spin splitting in altermagnets exhibits angular momentum structures classified by even harmonics such as  $d$ -wave ( $l = 2$ ),  $g$ -wave ( $l = 4$ ), and  $i$ -wave ( $l = 6$ ) [2, 8].

The theoretical predictions of altermagnetism have sparked intense experimental efforts. These led to the direct observation of giant spin splittings via angle-resolved photoemission spectroscopy (ARPES) in various candidate materials including MnTe [9–11], CrSb [12], and Mn<sub>5</sub>Si<sub>3</sub> [13]. Consequently, the interplay between this unconventional magnetic order and the underlying crystal symmetry generates a rich variety of transport phenomena. Experimental and theoretical studies have reported the anomalous Hall effect [3, 14, 15, 17], the spin-splitter effect [18–20], and novel magnetoresistance behaviors [21–23].

Beyond linear transport, nonlinear responses offer powerful probes of geometric and topological properties in quantum materials. In the electrical domain, the second-order nonlinear Hall effect has been extensively studied, primarily driven by two intrinsic geometric quantities. These are the Berry curvature dipole [24–27] and the Berry connection polarizability (BCP) [28–32]. In systems with combined  $\mathcal{PT}$  symmetry where the Berry curvature vanishes, the BCP provides the leading intrinsic contribution to the nonlinear Hall signal [29, 30, 33]. The BCP is intrinsically linked to the quantum metric [45, 46].

Recently, the discovery of a large magnetic nonlinear Hall effect (MNLHE) in the  $d$ -wave altermagnet Mn<sub>5</sub>Si<sub>3</sub> [16] has demonstrated that nonlinear electrical transport serves as a sensitive experimental signature of altermagnetic symmetry breaking [34–36]. Despite rapid progress in the electrical domain, the extension of intrinsic non-

linear Hall physics to the thermal domain remains unexplored. While researchers have theoretically investigated the linear thermal Hall effect in altermagnets [37–39], the geometrical origin of the second-order nonlinear thermal Hall effect requires systematic clarification. The foundation for such geometric thermal transport relies on Luttinger’s formal prescription [40–44]. However, the explicit symmetry constraints for altermagnets have not been fully mapped out.

In this work, we provide a step-by-step framework that establishes the central symmetry selection rules for the intrinsic nonlinear thermal Hall effect in altermagnets. By detailing every derivation, we prove that the twofold rotational symmetry ( $C_2$ ) acts as the gatekeeper for macroscopic geometric thermal transport. This explains why materials like Mn<sub>5</sub>Si<sub>3</sub> succeed where highly symmetric systems fail.

## II. MODEL FORMULATION AND QUANTUM METRIC DERIVATION

### A. Algebraic derivation of the quantum metric

We consider a time-reversal-symmetric two-band effective Hamiltonian:

$$H(\mathbf{k}) = \mathbf{g}(\mathbf{k}) \cdot \boldsymbol{\sigma} = g_x(\mathbf{k})\sigma_x + g_z(\mathbf{k})\sigma_z, \quad (1)$$

where we set  $g_y = 0$ . The band energies are  $\epsilon_{\pm}(\mathbf{k}) = \pm G(\mathbf{k})$  with  $G = \sqrt{g_x^2 + g_z^2}$ .

The quantum metric  $g_{ab}$  captures the geometric distance between neighboring Bloch states. We start from the general expression [45]:

$$g_{ab} = \frac{1}{4G^4} [G^2(\partial_a \mathbf{g} \cdot \partial_b \mathbf{g}) - (\mathbf{g} \cdot \partial_a \mathbf{g})(\mathbf{g} \cdot \partial_b \mathbf{g})]. \quad (2)$$

We explicitly evaluate the inner products for our two-component vector  $\mathbf{g} = (g_x, 0, g_z)$ . First, the scalar product of derivatives is  $\partial_a \mathbf{g} \cdot \partial_b \mathbf{g} = \partial_a g_x \partial_b g_x + \partial_a g_z \partial_b g_z$ . Second, the product between the vector and its derivative is  $\mathbf{g} \cdot \partial_a \mathbf{g} = g_x \partial_a g_x + g_z \partial_a g_z$ . Substituting these

into the numerator and expanding the energy gap term  $G^2 = g_x^2 + g_z^2$ , we obtain:

$$\begin{aligned} \text{Num} = & (g_x^2 + g_z^2)(\partial_a g_x \partial_b g_x + \partial_a g_z \partial_b g_z) \\ & - (g_x \partial_a g_x + g_z \partial_a g_z)(g_x \partial_b g_x + g_z \partial_b g_z). \end{aligned} \quad (3)$$

We expand the brackets to identify the canceling terms. The expanded numerator is:

$$\begin{aligned} \text{Num} = & g_x^2 \partial_a g_x \partial_b g_x + g_x^2 \partial_a g_z \partial_b g_z + g_z^2 \partial_a g_x \partial_b g_x \\ & + g_z^2 \partial_a g_z \partial_b g_z - g_x^2 \partial_a g_x \partial_b g_x - g_x g_z \partial_a g_x \partial_b g_z \\ & - g_z g_x \partial_a g_z \partial_b g_x - g_z^2 \partial_a g_z \partial_b g_z. \end{aligned} \quad (4)$$

The terms  $g_x^2 \partial_a g_x \partial_b g_x$  and  $g_z^2 \partial_a g_z \partial_b g_z$  cancel exactly. The surviving terms are:

$$\begin{aligned} \text{Num} = & g_x^2 \partial_a g_z \partial_b g_z + g_z^2 \partial_a g_x \partial_b g_x \\ & - g_x g_z (\partial_a g_x \partial_b g_z + \partial_a g_z \partial_b g_x). \end{aligned} \quad (5)$$

We now verify that this equals the factored form  $(g_z \partial_a g_x - g_x \partial_a g_z)(g_z \partial_b g_x - g_x \partial_b g_z)$ . Expanding the product gives  $g_z^2 \partial_a g_x \partial_b g_x - g_z g_x \partial_a g_x \partial_b g_z - g_x g_z \partial_a g_z \partial_b g_x + g_x^2 \partial_a g_z \partial_b g_z$ , which matches term by term. Therefore, the quantum metric takes the compact form:

$$g_{ab} = \frac{(g_z \partial_a g_x - g_x \partial_a g_z)(g_z \partial_b g_x - g_x \partial_b g_z)}{4(g_x^2 + g_z^2)^2}. \quad (6)$$

This derivation shows that a non-zero  $g_{ab}$  strictly requires interband coupling driven by orbital mixing or spin-orbit coupling.

### B. *d*-wave altermagnet

Motivated by the orthorhombic phase of  $\text{Mn}_5\text{Si}_3$  [15], we construct the *d*-wave exchange splitting on a square lattice:

$$g_z(\mathbf{k}) = \Delta(\cos k_x - \cos k_y). \quad (7)$$

To generate a nontrivial quantum metric, we introduce an interband coupling consisting of a parity-even orbital mixing term and a parity-odd spin-orbit coupling term:

$$g_x(\mathbf{k}) = 2t_1 \sin k_x \sin k_y + \lambda \sin k_y. \quad (8)$$

### C. True 2D *g*-wave altermagnet and the $O(k^4)$ proof

To properly contrast the *d*-wave case, we construct a mathematically rigorous 2D *g*-wave model on the same square lattice:

$$g_z(\mathbf{k}) = \Delta \sin k_x \sin k_y (\cos k_x - \cos k_y). \quad (9)$$

We define the interband coupling as  $g_x(\mathbf{k}) = \lambda \sin k_y$ . We prove the *g*-wave nature by performing a Taylor expansion around the  $\Gamma$  point. The sine terms expand as

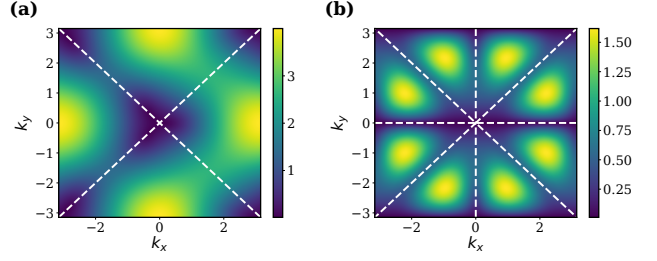


FIG. 1. Comparison of the energy gap  $2G(\mathbf{k})$  and nodal lines (white dashed lines). (a) The *d*-wave model forms nodal lines along  $k_x = \pm k_y$ . (b) The *g*-wave model possesses a complex eightfold nodal structure. Parameters:  $\Delta = 1.0$ ,  $t_1 = 0.5$ ,  $\lambda = 0.3$ .

$\sin k_x \approx k_x$  and  $\sin k_y \approx k_y$ . The cosine difference expands as follows:

$$\cos k_x - \cos k_y \approx (1 - k_x^2/2) - (1 - k_y^2/2) = -\frac{1}{2}(k_x^2 - k_y^2). \quad (10)$$

We transform the momentum to polar coordinates where  $k_x = k \cos \theta$  and  $k_y = k \sin \theta$ . We evaluate the product:

$$\begin{aligned} g_z(\mathbf{k}) & \approx \Delta(k \cos \theta)(k \sin \theta) \left[ -\frac{1}{2}(k^2 \cos^2 \theta - k^2 \sin^2 \theta) \right] \\ & = -\frac{1}{2} \Delta k^4 (\cos \theta \sin \theta) (\cos 2\theta). \end{aligned} \quad (11)$$

We apply the trigonometric identity  $\sin 2\theta = 2 \sin \theta \cos \theta$ :

$$g_z(\mathbf{k}) \approx -\frac{1}{4} \Delta k^4 \sin 2\theta \cos 2\theta. \quad (12)$$

We apply the identity again to obtain the final result:

$$g_z(\mathbf{k}) \approx -\frac{1}{8} \Delta k^4 \sin 4\theta. \quad (13)$$

This step-by-step expansion guarantees that the leading term is exactly  $O(k^4)$  with a fourfold angular dependence. Crucially,  $g_z(-\mathbf{k}) = g_z(\mathbf{k})$ , which makes it a pure even function.

## III. SYMMETRY SELECTION RULES AND MATRIX PROOFS

### A. Mirror symmetry breaking

Under a mirror reflection  $M_x$  mapping  $x$  to  $-x$ , each spatial index  $x$  in the rank-3 tensor  $\kappa_{abc}$  acquires a factor of  $(-1)$ , so that  $\kappa_{abc} \rightarrow (-1)^{n_x} \kappa_{abc}$  where  $n_x$  counts the number of  $x$ -indices. Both our models break  $M_x$  through the  $\lambda \sin k_y$  term. Mirror symmetry  $M_y$  is preserved. This forces the components  $\kappa_{xxy}$ ,  $\kappa_{yxx}$ , and  $\kappa_{yyy}$  to vanish. This restriction leaves only  $\kappa_{xxx}$ ,  $\kappa_{xyy}$ , and  $\kappa_{yxy}$  as permissible.

## B. Algebraic proof of $C_2$ symmetry protection

Under a  $C_2$  rotation ( $\mathbf{k} \rightarrow -\mathbf{k}$ ), every spatial index acquires a minus sign, so that  $\kappa_{abc} \rightarrow (-1)^3 \kappa_{abc} = -\kappa_{abc}$ . If the Hamiltonian preserves  $C_2$ , the macroscopic transport coefficient must obey  $\kappa_{abc} \equiv 0$ . The physical  $C_2$  rotation acts as  $\mathbf{k} \rightarrow -\mathbf{k}$  in momentum space. We use a pseudospin representation  $U = \sigma_z$ . This representation preserves the  $\sigma_z$  intermagnetic splitting channel while flipping the  $\sigma_x$  interband coupling channel. We test the unitary operator as follows:

$$\begin{aligned} \sigma_z H(\mathbf{k}) \sigma_z &= \sigma_z (g_x(\mathbf{k}) \sigma_x + g_z(\mathbf{k}) \sigma_z) \sigma_z \\ &= g_x(\mathbf{k}) (\sigma_z \sigma_x \sigma_z) + g_z(\mathbf{k}) (\sigma_z \sigma_z \sigma_z). \end{aligned} \quad (14)$$

We apply the Pauli matrix identities  $\sigma_z \sigma_x \sigma_z = -\sigma_x$  and  $\sigma_z \sigma_z \sigma_z = \sigma_z$ . We find:

$$\sigma_z H(\mathbf{k}) \sigma_z = -g_x(\mathbf{k}) \sigma_x + g_z(\mathbf{k}) \sigma_z. \quad (15)$$

For the  $g$ -wave model,  $g_z(-\mathbf{k}) = g_z(\mathbf{k})$  and  $g_x(-\mathbf{k}) = -g_x(\mathbf{k})$ . The Hamiltonian at the inverted momentum is  $H(-\mathbf{k}) = g_x(-\mathbf{k}) \sigma_x + g_z(-\mathbf{k}) \sigma_z = -g_x(\mathbf{k}) \sigma_x + g_z(\mathbf{k}) \sigma_z$ . Comparing this result with Eq. (15), we find the exact equivalence  $\sigma_z H(\mathbf{k}) \sigma_z = H(-\mathbf{k})$ . The  $g$ -wave system perfectly preserves  $C_2$  symmetry. It mathematically forces  $\kappa_{xyy} = 0$ . In contrast, the  $d$ -wave model contains a parity-even term ( $2t_1 \sin k_x \sin k_y$ ) in  $g_x(\mathbf{k})$ . This means  $g_x(-\mathbf{k}) \neq \pm g_x(\mathbf{k})$ , the unitary equivalence breaks down,  $C_2$  is broken, and  $\kappa_{xyy}$  survives.

## IV. FORMALISM AND INTEGRATION BY PARTS

We employ Luttinger's formal prescription to relate the thermal transport coefficient to the electrical Berry connection polarizability (BCP)  $\mathcal{G}_{xy}^{(n)} = n g_{xy} / (2G)$  [28, 40]. The substitution  $e\mathbf{E} \rightarrow \frac{\epsilon - \mu}{T} \nabla T$  maps the electrical nonlinear Hall conductivity onto its thermal counterpart. This formal correspondence is rigorously established in the linear regime by Luttinger [40] and Qin, Niu, and Shi [41]. In the nonlinear regime, the analogous electrical BCP formula has been experimentally validated [33]. A fully rigorous quantum kinetic theory incorporating magnetization current corrections [41, 42] and second-order positional shifts remains an open challenge. We focus here on the leading-order geometric contributions which dominate the symmetry-protected transport bounds.

The raw integral takes the form:

$$\kappa_{xyy} = \frac{1}{\hbar T^2} \int_{\text{BZ}} \frac{d^2 k}{(2\pi)^2} \sum_n W(\epsilon_n) \partial_{k_y} \mathcal{G}_{xy}^{(n)}, \quad (16)$$

where  $W(\epsilon) = (\epsilon - \mu)^2 f_0(\epsilon)$  represents the thermal weight. Near the nodal lines where the energy gap approaches zero, the polarizability behaves as  $\mathcal{G}_{xy} \propto 1/G^3$  and its derivative scales as  $1/G^4$ , as can be seen directly

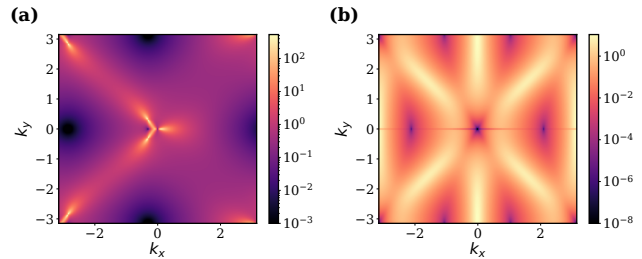


FIG. 2. Distribution of the trace of the quantum metric,  $\text{Tr}(g_{ab})$ . (a)  $d$ -wave and (b)  $g$ -wave models form geometric hotspots near nodal lines. These singular structures, shown on a logarithmic scale, act as the source for macroscopic transport. Parameters:  $\Delta = 1.0$ ,  $t_1 = 0.5$ ,  $\lambda = 0.3$ .

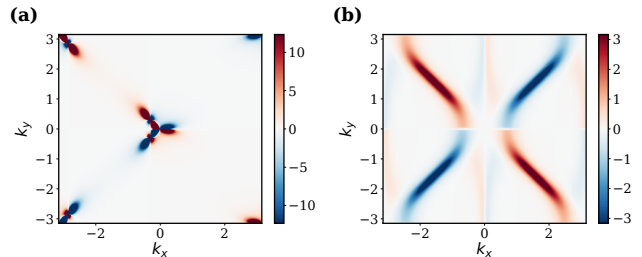


FIG. 3. Contrast in the symmetry of the Berry connection polarizability  $\mathcal{G}_{xy}$ . (a) The asymmetric texture of  $d$ -wave indicates  $C_2$  breaking. (b) The perfectly antisymmetric structure of  $g$ -wave visually proves the protection by  $C_2$  symmetry. This point-symmetric structure forces the global integral to vanish. Parameters:  $\Delta = 1.0$ ,  $t_1 = 0.5$ ,  $\lambda = 0.3$ .

from Eq. (6). We tame this mathematical singularity by performing integration by parts over the Brillouin zone:

$$\int (\partial_{k_y} \mathcal{G}_{xy}) W(\epsilon) d^2 k = - \int \mathcal{G}_{xy} (\partial_{k_y} W(\epsilon)) d^2 k. \quad (17)$$

We apply the chain rule  $\partial_{k_y} = \hbar v_y \partial_\epsilon$ . We expand the energy derivative of the thermal weight using the product rule:

$$\frac{\partial W(\epsilon)}{\partial \epsilon} = 2(\epsilon - \mu) f_0(\epsilon) + (\epsilon - \mu)^2 f_0'(\epsilon). \quad (18)$$

Substituting this expansion back into the transport equation yields the robust and divergence-free formula:

$$\kappa_{xyy} = - \frac{1}{\hbar T^2} \int_{\text{BZ}} \frac{d^2 k}{(2\pi)^2} \sum_n \mathcal{G}_{xy}^{(n)} W_n'(\epsilon) v_{y,n}. \quad (19)$$

This step-by-step unrolling shifts the derivative onto the smooth Fermi-Dirac distribution.

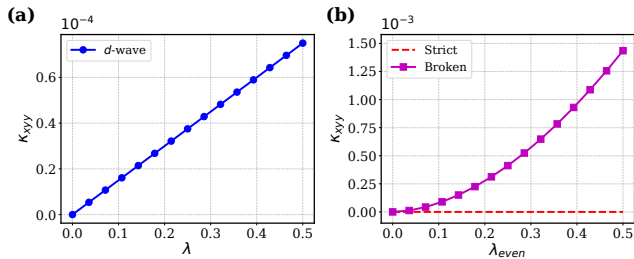


FIG. 4. Numerical evaluation of the nonlinear thermal Hall conductivity  $\kappa_{xyy}$ . (a) The  $d$ -wave model displays a linear increase with the parameter  $\lambda$ . (b) The  $g$ -wave model stays exactly at zero when  $C_2$  is preserved (dashed line). The signal recovers sharply when  $C_2$  is broken (solid line with squares). Parameters:  $\Delta = 1.0$ ,  $\mu = -0.5$ ,  $T = 0.05$ ,  $\eta = 0.005$ ;  $t_1 = 0.5$  for  $d$ -wave.

## V. ANALYTICAL SCALING AND NUMERICAL RESULTS

### A. Analytical scaling relation

We extract the parametric dependence of the conductivity for the  $d$ -wave model. We expand the product of derivatives  $\varphi_x\varphi_y$  to first order in the symmetry-breaking parameter  $\lambda$ . This reveals the relation  $\varphi_x\varphi_y \approx \mathcal{F}(\mathbf{k}) \cdot (\lambda\Delta t_1)$ . Since the function  $\mathcal{F}(\mathbf{k})$  is a parity-even function of momentum, it survives the Brillouin zone integration without cancellation. This results in the linear scaling law  $\kappa_{xyy} \propto \lambda\Delta t_1$ .

### B. Numerical verification

We compute  $\kappa_{xyy}$  using adaptive sub-grid patching to resolve nodal singularities. The parameters are  $\Delta = 1.0$ ,  $t_1 = 0.5$ ,  $\mu = -0.5$ ,  $T = 0.05$ , and broadening  $\eta = 0.005$ .

For the  $d$ -wave model,  $\kappa_{xyy}$  exhibits a clean, monotonic linear dependence on the mirror-breaking parameter  $\lambda$  [Fig. 4(a)], confirming the analytically derived scaling.

The  $g$ -wave model results [Fig. 4(b)] serve as the nu-

merical proof of our symmetry theorem. When  $C_2$  is preserved ( $\lambda_{\text{even}} = 0$ ),  $\kappa_{xyy}$  remains locked at numerical zero ( $\sim 10^{-19}$ ). Immediately upon introducing an even-parity,  $C_2$ -breaking term to the interband coupling ( $\lambda_{\text{even}} \neq 0$ ), a robust geometric signal is recovered, increasing monotonically to match the scale of the  $d$ -wave response.

## VI. CONCLUSION

We have established the fundamental selection rules for the intrinsic nonlinear thermal Hall effect driven by the quantum metric in altermagnets. The twofold rotational symmetry ( $C_2$ ) acts as the primary gatekeeper for the macroscopic geometric response. Through rigorous mathematical derivations and numerical verification, we demonstrated that  $d$ -wave materials naturally generate a finite signal by breaking this rotational protection, while  $g$ -wave systems preserve  $C_2$  symmetry and extinguish the geometric signal.

We emphasize the generality of our central result. The  $C_2$  selection rule is lattice-independent: it is a consequence of point-group symmetry acting on a rank-3 tensor, valid for any lattice geometry including the hexagonal structures of actual  $g$ -wave altermagnets such as CrSb and NiS. Whether a specific material preserves or breaks  $C_2$  depends on the microscopic details of the spin-orbit coupling, which must be determined by first-principles calculations for each candidate.

These selection rules provide a diagnostic tool for current experimental controversies. If ideal RuO<sub>2</sub> with a pristine rutile structure preserves  $C_2$  symmetry, the intrinsic nonlinear thermal Hall effect must be zero [2]. A finite observed signal would provide evidence of hidden symmetry breaking such as spin canting or defect-induced strain. Conversely, Mn<sub>5</sub>Si<sub>3</sub> is an optimal platform among  $d$ -wave altermagnets for observing these geometric responses, because its orthorhombic distortion below the Néel temperature naturally breaks  $C_2$  [15, 16]. Our results clarify the microscopic origin of nonlinear thermal transport and provide guidelines for designing spin-caloritronic devices.

- 
- [1] L. Šmejkal, J. Sinova, and T. Jungwirth, Phys. Rev. X **12**, 031042 (2022).
  - [2] L. Šmejkal, J. Sinova, and T. Jungwirth, Phys. Rev. X **12**, 040501 (2022).
  - [3] L. Šmejkal *et al.*, Sci. Adv. **6**, eaaz8809 (2020).
  - [4] I. I. Mazin *et al.*, Phys. Rev. X **12**, 041005 (2022).
  - [5] I. I. Mazin, Phys. Rev. B **107**, L100418 (2023).
  - [6] S. Hayami *et al.*, J. Phys. Soc. Jpn. **88**, 123702 (2019).
  - [7] J. Ahn *et al.*, Phys. Rev. B **99**, 184432 (2019).
  - [8] L. Šmejkal *et al.*, Nature **605**, 261 (2022).
  - [9] J. Krempaský *et al.*, Nature **626**, 517 (2024).
  - [10] S. Lee *et al.*, Phys. Rev. Lett. **132**, 036401 (2024).
  - [11] T. Osumi *et al.*, Phys. Rev. B **109**, 115147 (2024).
  - [12] S. Reimers *et al.*, Nat. Commun. **15**, 2116 (2024).
  - [13] J. Krempaský *et al.*, arXiv:2404.14589 (2024).
  - [14] Z. Feng *et al.*, Nat. Electron. **5**, 735 (2022).
  - [15] H. Reichlová *et al.*, arXiv:2402.13268 (2024).
  - [16] L. Han *et al.*, arXiv:2502.04920 (2025).
  - [17] R. D. Betancourt *et al.*, Phys. Rev. Lett. **130**, 036702 (2023).
  - [18] R. González-Hernández *et al.*, Phys. Rev. Lett. **130**, 046702 (2023).
  - [19] D.-F. Shao *et al.*, Phys. Rev. B **109**, 094411 (2024).
  - [20] H. Bai *et al.*, Phys. Rev. Lett. **131**, 056701 (2023).

- [21] T. Hajlaoui *et al.*, arXiv:2403.01869 (2024).
- [22] X. Zhou *et al.*, Phys. Rev. B **109**, 104423 (2024).
- [23] X. Chen *et al.*, Phys. Rev. B **109**, 054432 (2024).
- [24] I. Sodemann and L. Fu, Phys. Rev. Lett. **115**, 216806 (2015).
- [25] Q. Ma *et al.*, Nature **565**, 337 (2019).
- [26] K. Kang *et al.*, Nat. Mater. **18**, 324 (2019).
- [27] Z. Z. Du *et al.*, Nat. Rev. Phys. **3**, 744 (2021).
- [28] Y. Gao *et al.*, Phys. Rev. Lett. **112**, 166601 (2014).
- [29] H. Liu *et al.*, Phys. Rev. Lett. **127**, 277202 (2021).
- [30] C. Wang *et al.*, Phys. Rev. B **108**, 045105 (2023).
- [31] A. Lau *et al.*, Phys. Rev. Lett. **126**, 036803 (2021).
- [32] D. Kaplan *et al.*, Phys. Rev. Lett. **132**, 026301 (2024).
- [33] A. Gao *et al.*, Nature **620**, 533 (2023).
- [34] X. Wang *et al.*, Phys. Rev. Lett. **132**, 116301 (2024).
- [35] Y. Zhang *et al.*, Phys. Rev. B **109**, 085122 (2024).
- [36] Y. Gao *et al.*, Nat. Commun. **15**, 350 (2024).
- [37] A. Bose *et al.*, Phys. Rev. B **105**, 014401 (2022).
- [38] X. Zhou *et al.*, Phys. Rev. B **109**, 144415 (2024).
- [39] Y. Mokrousov *et al.*, arXiv:2401.07789 (2024).
- [40] J. M. Luttinger, Phys. Rev. **135**, A1505 (1964).
- [41] T. Qin, Q. Niu, and J. Shi, Phys. Rev. Lett. **107**, 236601 (2011).
- [42] D. Xiao *et al.*, Phys. Rev. Lett. **97**, 026603 (2006).
- [43] X.-Q. Yu *et al.*, Phys. Rev. B **100**, 155141 (2019).
- [44] C. Zeng *et al.*, Phys. Rev. B **105**, 075133 (2022).
- [45] J. P. Provost and G. Vallee, Commun. Math. Phys. **76**, 289 (1980).
- [46] R. Resta, Eur. Phys. J. B **79**, 121 (2011).